Performance Analysis of Digital Filtering Algorithms in Energy Reconstruction for the ATLAS Liquid Argon Calorimeter

Author: Claire Yang
Supervisor: Brigitte Vachon, Alessandro Ambler

Abstract

In this study, we explored and evaluated various digital filtering algorithms for energy reconstruction in the ATLAS LAr calorimeter with future readout electronics. The Optimal Filter (OF) and Least-Squares Finite Impulse Response (LS-FIR) filters were tested on two datasets, the Electromagnetic Barrel (EMB) and Hadronic End-cap (HEC) data. We analyzed the mean, median, and standard deviation of the residuals with respect to true energy to assess filter performance. Our results indicate that the LS-FIR filters exhibit more balanced performance across different scenarios, while the OF excels in reconstructing sparse delta function signals. The choice of filter should be tailored to the characteristics of the data. Furthermore, we compared the LS-FIR filters with Convolutional Neural Network (CNN) models, and found that higher-order FIR filters perform competitively with the CNN models in certain cases.

1. Introduction

The High-Luminosity Large Hadron Collider (LHC) [3] is expected to revolutionize our understanding of the Universe's fundamental properties. However, the significantly increased luminosity and consequently, the increased number of particle interactions, rise challenges to accurate signal detection and energy reconstruction. One of the challenges is due to the pileup noise leading by overlapping signals that can seriously affect the fidelity of energy measurements. The current energy reconstruction method based on the Optimal Filter with 4 coefficients has been sufficient for past LHC runs [1]. It's evident that under the demanding conditions of high luminosity, an upgraded approach is necessary.

The ATLAS detector comprises multiple subsystems designed to measure various particle properties[5]. Among these, the Electromagnetic Barrel calorimeter (EMB) is designed to measure energies of electrons and photons as they interact predominantly via the electromagnetic force. On the other hand, the Hadronic End-cap Calorimeter (HEC) measures the energy of hadrons interacting predominantly through the strong force. Both the EMB and HEC are playing important roles for the accurate measurement of energy deposition from particle collisions. However, the unique characteristics and challenges associated with each calorimeter underscore the need for tailored digital filtering techniques for optimal energy reconstruction.

In this project, we mainly working on the exploration, implementation, and detailed performance evaluation of diverse digital filtering algorithms tailored for the ATLAS LAr calorimeter's future readout electronics. The overarching goal is to find a digital filter that ensures peak energy reconstruction fidelity, especially in the environment of the High-Luminosity LHC.

2. Method

2.1 Dataset Description

2.1.1 Signal Formation and ADC Output

The primary signal, E_{true}, simulated for this study is composed of two integral components: a delta function signal and the pileup noise, simulating extraneous particle interactions. The Analog-to-Digital Converter output (ADC), which emulates the readout electronics system of the ATLAS detector, processes this true signal. Formally, the ADC output data can be represented as:

$$\boldsymbol{d} = H * \boldsymbol{s} + \boldsymbol{n} \tag{1}$$

where H is the time response function, convolved with the true signal $\boldsymbol{s} = E_{\text{true}} = E_{\text{signal}} + E_{\text{pileup}}$. Here, $\boldsymbol{n}$ signifies the inherent noise associated with the measurements.

An illustration of the pulse shape is provided in Figure 1. Each pulse spans over 20 Bunch Crossing (BC) intervals (every 25 ns).

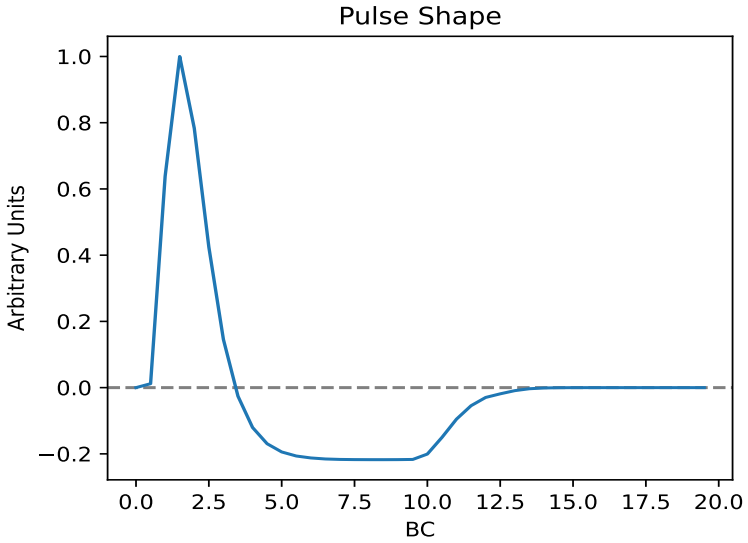

Figure 1: The typical pulse shape captured in the ATLAS detector.

2.1.2 HEC Data

The HEC dataset was constructed with signals injected at random frequencies atop raw signals. With an average interaction number (μ) of 200 per bunch crossing, the dataset encompasses a total of 1,000,000 data points. To mitigate edge effects and ensure data integrity, the first and last 10,000 data points were excluded from the analysis.

2.1.3 EMB Data

The EMB dataset we utilized is from the middle layer of the ATLAS Electromagnetic Calorimeter. Various datasets were generated based on the spatial coordinates given by pseudorapidity η and azimuthal angle ϕ, with values 0.5125 and 0.0125 respectively. The μ value is 140 in our datasets. One EMB dataset has 22,000,000 data points, and we cut the first and last 1,000,000 data points when appling the filters.

The EMB dataset encompasses various signal conditions, segmented into five categories: `OnlyPileup` which exemplifies the background noise by containing only the pileup; `ConstGapLowE` layering a consistent low-energy signal atop the pileup with signals introduced at a uniform frequency; `RdGapLowE` distinct for its sporadic nature with low-energy signals introduced at irregular intervals, occasionally leading to signal overlap; `ConstGapHighE` analogous to `ConstGapLowE` but with elevated signal energy levels, having high-energy signals introduced at regular intervals; `RdGapHighE` notable for the presence of high-energy signals introduced intermittently, resulting in a dynamic signal pattern. This categorization aids in analyzing how different filters perform under varied signal conditions and complexities in the EMB dataset.

2.2 Digital Filter Design

The primary methods employed in this study are the Optimal Filter (OF) and various Finite Impulse Response (FIR) filters designed using a least-squares approach.

2.2.1 Optimal Filter (OF)

The Optimal Filter utilizes a set of coefficients specifically curated for the unique system response and the signal features we aim to extract. For the HEC dataset, the OF employs 4 coefficients, corresponding to those outlined in the introduction. Meanwhile, for the EMB dataset, 16 predetermined coefficients are used. The underpinning logic of the OF is to mitigate noise effects and retrieve pivotal signal parameters, such as amplitude and initiation time. This is facilitated by resolving a least squares problem, wherein the noise's influence on the signal is minimized. A comprehensive elucidation of this technique is provided in Cleland's work [4]. In this study, the OF mainly serves as a reference to benchmark the efficacy of our other filters.

2.2.2 Least Squares Finite Impulse Response Filters (LS-FIR)

For the LS-FIR filter, our approach involves direct least-squares estimation of the filter coefficients using the input signal and simulated detector outputs.

The usual least-squares problem for data with structure as Eqn.1 is:

$$\nabla\chi^2 = -2H^T N^{-1}(\boldsymbol{d} - H * \boldsymbol{s}) = 0,$$

which can be formulated as $\mathbf{s} = D\mathbf{c}$, where $N_{ij} =< n_i n_j >$ denotes the noise matrix, $\mathbf{c}$ signifies the filter coefficients, and D is a design matrix constructed from the data $\boldsymbol{d}$. The least-squares solution is:

$$\mathbf{c} = (D^T D)^{-1} D^T \boldsymbol{s}$$

The derivation of the least-squares FIR filter can be extended easily to non-linear FIR filters. A simple yet highly effective filter model involves including powers of the data:

$$s_i = \sum_{j=-n_{left}}^{n_{right}} c_0 + c_1, j \cdot d_{i+j} + c_2, j \cdot d_{i+j}^2 + \dots$$

Thus, data squared (and cubed, etc.) is now also fed into the filter. The output, while nonlinear in the data, remains linear with respect to the filter coefficients and exhibits a finite response.

Here we analyzed the linear,quadratic and cubic filter, with the sliding window encompasses $n_{left} = 30$ data points to the left and $n_{right} = 8$ to the right, totaling 39 coefficients for the filter.

2.3 Evaluation Method

An essential part of our methodology focuses on the evaluation of the filtering techniques. We employ two principal metrics to assess the filter performance: residual distribution analysis and error analysis.

The residuals are calculated as the differences between the reconstructed signal and the true signal $\Delta E = E_{\text{reco}} - E_{\text{true}}$. We categorize the residual data into ten distinct bins according to the range of E_{true}, and examine the mean, median within 98% of data, standard deviation (Stdev), and relative Stdev (residual standard deviation to E_{true}) within each bin.

While the above metric offers a view of filter performance across different signal levels, a more holistic assessment can be gleaned from evaluating the global standard deviation of the residuals.

Furthermore, to gauge the filters' efficiency in an almost noise-free environment, we compute the ideal error. This metric corresponds to the standard deviation one would expect if the signal were isolated, i.e., in the absence of other overlapping signals. The ideal

error provides insights into the best achievable accuracy given the inherent limitations of the system and the noise model, and is calculated by $\sqrt{\frac{N}{h^T h}}$. The noise matrix $N = \boldsymbol{n}^T \boldsymbol{n} = (\boldsymbol{d} - H * \boldsymbol{s})^2$, and h is the detector response function, which takes as the filter coefficients.

3. Results

3.1 Results for HEC

3.1.1 Error Analysis

The following table 1 presents the observed error for various filtering techniques for the HEC dataset. According to the table, the LS-FIRs has smaller overall standard deviation than the OF, while if there is only one single signal, the OF gives the smallest ideal error.

Table 1: Error results for different filters on HEC dataset

Filter Type	Error (all BCID)	Ideal Error (single signal)
Optimal Filter	0.1175	0.0153
Linear FIR Filter	0.0463	0.6044
Quadratic FIR Filter	0.0426	0.2360
Cubic FIR Filter	0.0414	0.3781

There is another ideal error value of 0.0525 computed from the analysis, which represents the minimal reconstruction error achievable under conditions when only a primary signal is present. It quantifies the normalized reconstruction error by considering the entire energy of the signal in relation to the variance of the noise or error. Contrasting this with the ideal errors computed for individual filters, the latter often take into account specific filter characteristics or constraints. The 0.0525 value offers a more holistic and unconstrained view of the theoretical lower bound for error, without the influence of specific filter behaviors or limitations.

3.1.2 Residual Distribution Analysis

Based on the observations Fig. 2, the LS-FIR filters, especially the cubic and quadratic ones, work better than the OF in terms of standard deviation. While the OF tends to have a negative bias on mean and median. The relative standard deviation is likely to have a pattern reminiscent of exponential decay. Intriguingly, both the OF and the linear FIR present extremely large standard deviations for the first two energy intervals. In these two intervals, E_{true} is dominant by the pileup noise. The higher-order FIR filters like cubic and quadratic, may better capture the intricacies of the signal due to their multi-coefficient design

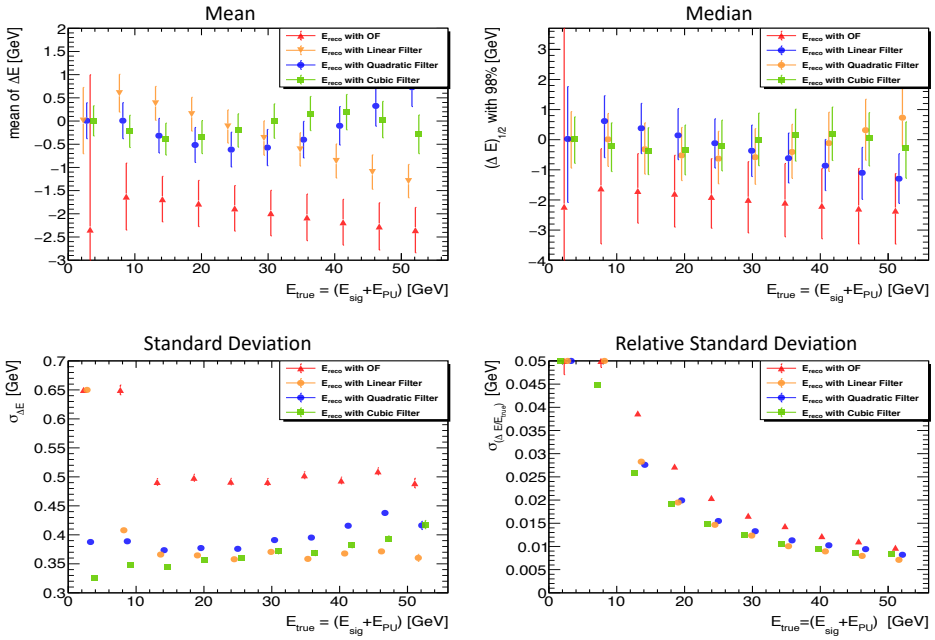

Figure 2: Residual distribution for HEC dataset.

3.2 EMB Data Results

3.2.1 Error Analysis

Table 2: Error for All BCID with EMB dataset.

Filter	OnlyPileup	ConstGapLowE	RdGapLowE	ConstGapHighE	RdGapHighE
Optimal	0.1175	1.5169	1.8415	12.1115	14.7173
Linear FIR	0.0463	0.2434	0.2689	0.8101	1.0372
Quadratic FIR	0.0426	0.1544	0.1840	0.4019	0.5802
Cubic FIR	0.0414	0.1335	0.1761	0.3169	0.4699

Table 3: Ideal Error for Single Signal with EMB dataset.

Filter	OnlyPileup	ConstGapLowE	RdGapLowE	ConstGapHighE	RdGapHighE
Optimal	0.0153	0.0778	0.0863	0.2197	0.2441
Linear FIR	0.6044	0.3107	0.3291	0.5511	0.4666
Quadratic FIR	0.2360	0.3928	0.3310	0.5113	0.5805
Cubic FIR	0.3781	0.5184	0.5095	0.8726	0.7942

According to the overall standard deviation we collected in table 2, the increasing trend of errors can be clearly observed as we transition from low energy data to high energy data for all filters. This suggests that the data with higher energy pose more challenges to these filters. Furthermore, when we look at random frequency (RdGap) data, there is also an

increase in standard deviation. In the case of the OF at high energy scenarios, there is a significant standard deviation which is notably larger compared to other LS-FIR filters. Moreover, as the order of the LS-FIR filter becomes higher, the standard deviation appears to decrease.

For the ideal error scenario in table 3, the OF consistently showcases the smallest error. This can be attributed to that the Of coefficients are designed to minimize the mean squared error, making it exceptionally suitable for situations where an ideal response is known and targeted. As for the lLS-FIR filters, the ideal error doesn't necessarily decrease with increasing order. This might be due to the fact that higher order doesn't always translate to better approximation, especially when the inherent nature of the signal is not well-suited for a polynomial approximation. Interestingly, as we transition from low energy to high energy in the context of ideal errors, it's not necessarily the case that the error of the filters consistently increases.

3.2.2 Residual Distribution Analysis

Starting with the ΔE distribution of `onlyPileup` in Fig. 3, the standard deviation for the delta E distribution appears rather erratic. A notable observation is that non-linear filters outperform the others, with the mean and median level closer to zero. This suggests that these filters are better at accurately reconstructing the signal without substantial deviation.

In Fig. 4, the ΔE distribution of `RdGapLowE` behaves mirrors that of the HEC data. One striking feature is the OF's 98th percentile lower boundary, which skews significantly towards negative values. This indicates a propensity for the OF to underestimate the true value to a considerable extent. Given that the `RdGapHighE` demonstrates similar characteristics as Fig. 7 in the appendix.

The behaviors of filters on the `ConstGapHighE` dataset is in Fig. 5. Surprisingly, the OF works well in the reconstruction of the delta function signal part. It outperforms the other filters, suggesting a favorable alignment between the filter characteristics and this particular signal type. However, the LS-FIR filters, especially when handling high-amplitude signals, tend to struggle: the standard deviation increases with the amplitude of the signal. This rising standard deviation could be because these filters might not handle rapid transitions or sharp features effectively at higher amplitudes. Given that the `ConstGapLowE` demonstrates similar characteristics as Fig. 6 in the appendix.

4. Discussion

The analysis of the EMB and HEC dataset reveals a nuanced performance of the OF. While it demonstrates superior ability in reconstructing delta function signals, its effectiveness is seriously compromised in scenarios dominated by pileup. The substantial standard deviation exhibited by the OF in pileup reconstruction results in a pronounced overall error. This

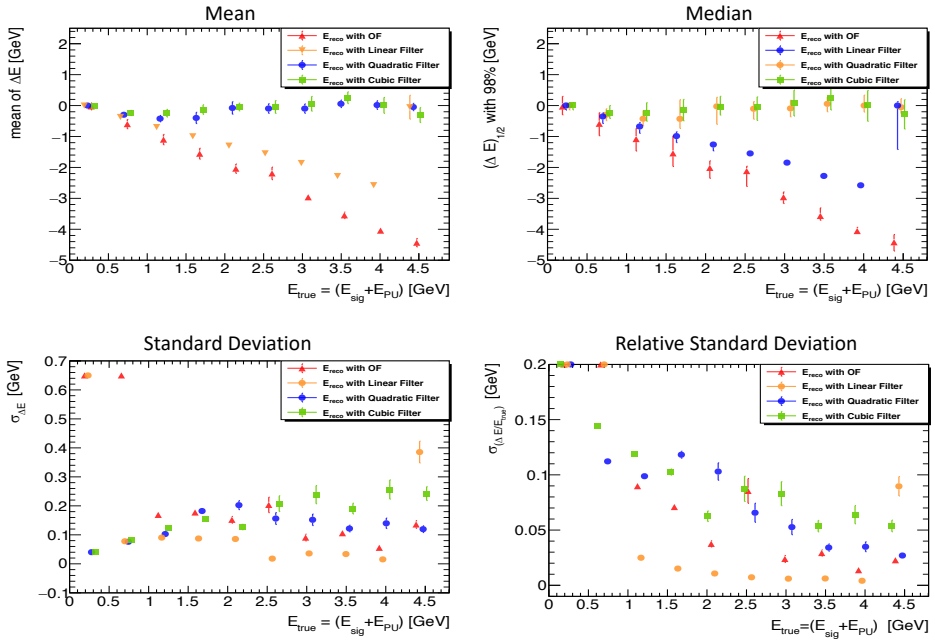

Figure 3: Residual distribution for the onlypile scenario.

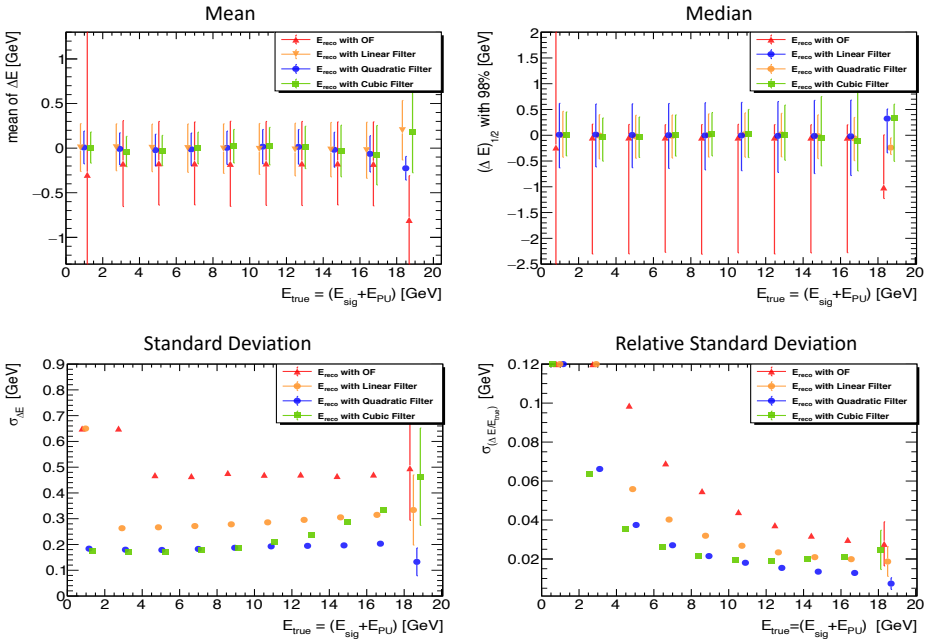

Figure 4: Residual distribution for `RdGapLowE` dataset.

suggests that the OF might not be the best choice for datasets where pileup is predominant, despite its excellence in more sparse and clear signal scenarios.

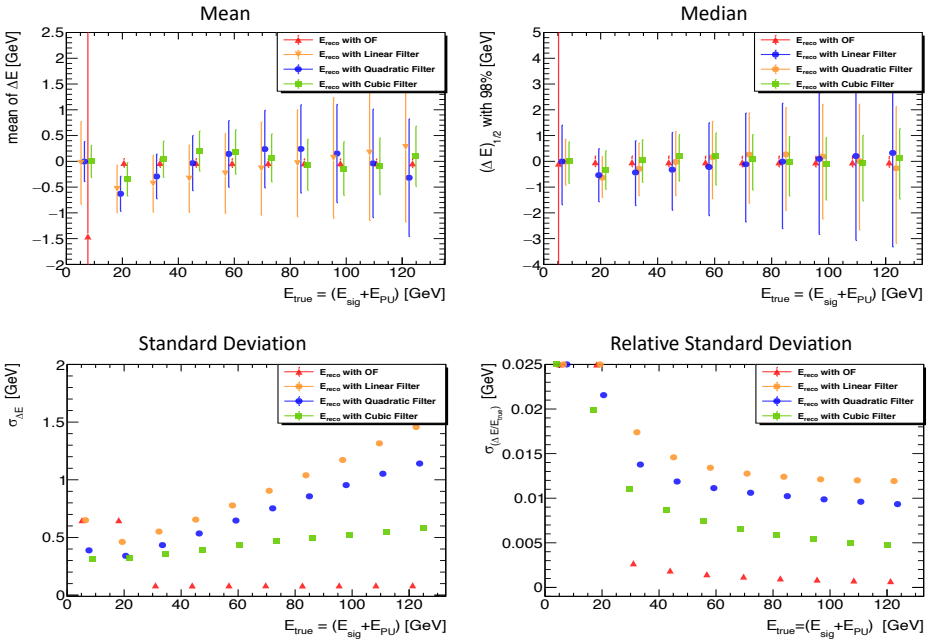

Figure 5: Residual distribution for `ConstGapHighE` dataset.

LS-FIR filters, on the other hand, show a more balanced performance across various datasets. Their errors don't spike as drastically as the OF in pileup dominated data, especially with higher orders. As the order increases, the standard deviation decreases, which can be a potential advantage in datasets with varied signal profiles.

Considering the varying performance of each filter across datasets, it's evident that there is no one-size-fits-all solution. The choice of filter needs to be tailored based on the characteristics of the data.

4.1 Comparison with Neural Network Based Approaches

In this section, we contrast the performance of our LS-FIR filters with two Convolutional Neural Network (CNN) based energy reconstruction models: a plain 2- to 3-layered CNN (2CNN) and a more complex 4-layered CNN with Tagging (4TCNN)[2].

All metrics for LS-FIR filters are normalized with respect to the OF performance, and compare the value of mean, median, and standard deviation ratio: $1 - X_{FIR}/X_{OF}$. Here we pick two high energy datasets with data points that have $E_{true} \in [1, 130]$GeV.

From the table, it's evident that: The LS-FIR filters, especially the higher-order ones, performs even better than the 2CNN and 4TCNN models on `rdGapHighE` dataset. The quadratic and cubic FIRs perform near or slightly better than CNN in terms of mean and median on `constGapHighE`.

Table 4: Comparison of LS-FIR filters and CNN models on the ‘rdGapHighE‘ dataset.

Model	**Mean [GeV]**	**Median [GeV]**	**StDev [GeV]**
Linear FIR	0.8663	0.8880	0.9362
Quadratic FIR	0.9903	1.0142	0.9627
Cubic FIR	0.9894	1.0091	0.9704
2CNN	0.8	0.94	-0.015
4TCNN	0.95	0.88	0.077

Table 5: Comparison of LS-FIR filters and CNN models on the ‘constGapHighE‘ dataset.

Model	**Mean [GeV]**	**Median [GeV]**	**StDev [GeV]**
Linear FIR	0.9228	-0.2648	0.9390
Quadratic FIR	0.9906	0.7664	0.9686
Cubic FIR	0.9864	0.8138	0.9749
2CNN	0.76	0.04	0.05
4TCNN	0.81	0.04	-0.04

5. Conclusion

In this study, we investigated digital filtering algorithms for energy reconstruction in the ATLAS LAr calorimeter. The LS-FIR filters offer a more versatile and robust approach for energy reconstruction, particularly in scenarios dominated by pileup noise. However, the Optimal Filter remains an excellent choice for sparse signals. We emphasize the importance of selecting the appropriate filter based on the specific characteristics of the data to achieve accurate and reliable energy reconstruction.

References

[1] ATLAS Liquid Argon Calorimeter Phase-II Upgrade: Technical Design Report. Technical report, CERN, Geneva, 2017. URL https://cds.cern.ch/record/2285582.

[2] Philipp Welle Anne-Sophie Berthold. Studies on convolutional neural networks for lar energy reconstruction. 2023.

[3] Oliver Brüning and Lucio Rossi. The high-luminosity large hadron collider. *Nature Reviews Physics*, 1(4):241–243, 2019. ISSN 2522-5820. doi: 10.1038/s42254-019-0050-6. URL https://doi.org/10.1038/s42254-019-0050-6.

[4] W. E. Cleland and E. G. Stern. Signal processing considerations for liquid ionization calorimeters in a high rate environment. *Nuclear Instruments and Methods in Physics Research A*, 338:467–497, 1993.

[5] Bertrand Laforge. The atlas liquid argon calorimeter: Construction, integration, commissioning. In *2006 IEEE Nuclear Science Symposium Conference Record*, volume 2, pages 885–890, 2006. doi: 10.1109/NSSMIC.2006.355989.

Appendix A. More Plots

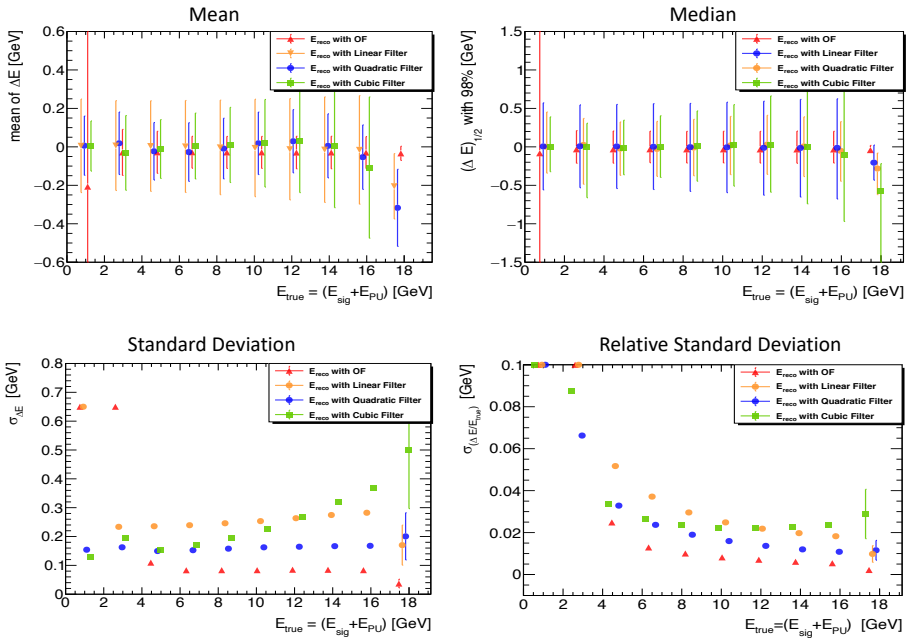

Figure 6: Residual distribution for `ConstGapLowE` dataset.

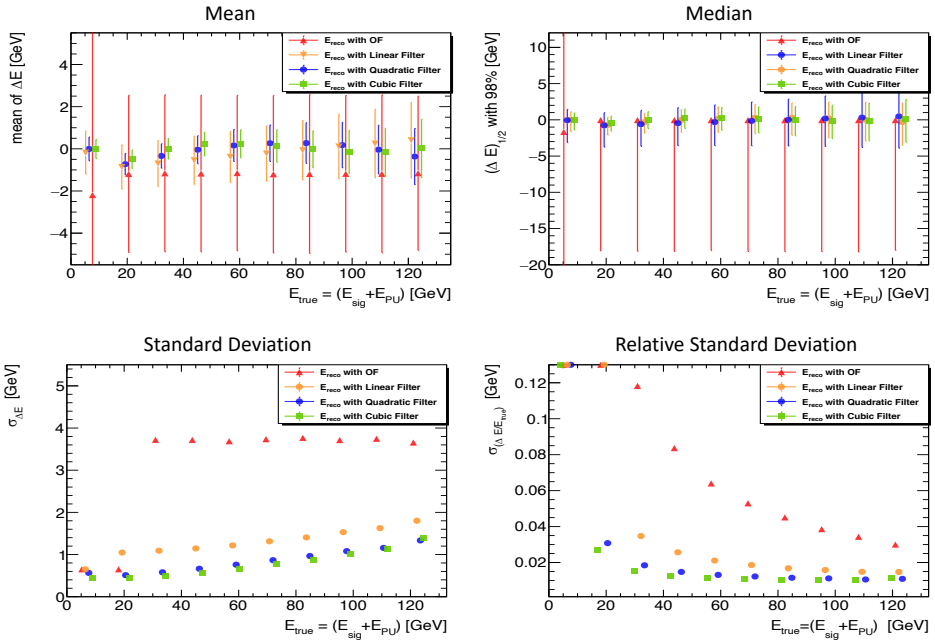

Figure 7: Residual distribution for `RdGapHighE` dataset.